Novel Characterization of Network Connectivity Changes Following Ischemia in Non-Human Primates

Bioengineering Capstone Report
BIOEN 402
06/02/2021

Shivalika Chavan
Neural Engineering & Rehabilitation Design (NERD) Lab
Dr. Azadeh Yazdan-Shahmorad, Departments of Bioengineering and Electrical & Computer Engineering
Karam Khateeb (PhD student in Bioengineering)

Abstract

Stroke is the leading cause of long-term disability in the United States. Disabilities can range from a loss of sensory function like touch, to motor functions like controlling arm movements due to the damage to the brain's network. Despite the prevalence of stroke, the underlying network dynamics that lead to functional deficits are not well understood. Due to the physiological similarities between non-human primate (NHP) and human brains, an NHP model is essential for studying the effects of stroke and developing stimulation-based therapies. Here we used the photothrombotic (PT) stroke technique to study network dynamics in the NHP sensorimotor cortex following an ischemic lesion. Using the PT stroke technique, we induced one focal ischemic lesion on the NHP sensorimotor cortex. We collected local field potentials from both hemispheres using an electrocorticographic (ECoG) array on the cortical surface. As a measure of local neural activity, we calculated ipsilesional power in the low gamma band, resulting in the formation of three clusters, characterized by their overall change (increase, decrease, no change) in power from baseline to three hours post-lesion. As expected, the cluster with an overall decrease in power corresponded to the lesion's physical location. We also studied the network connectivity by calculating pair-wise coherence across different frequency bands: theta, beta, low gamma, and high gamma. Overall, we saw that low frequencies were associated with decreases in coherence, while higher frequencies were associated with increases, with similar results from the contralesional hemisphere. In this study, we observed local neurophysiological changes up to three hours following an ischemic lesion. The observed increases in power in the perilesional region and coherence at high frequencies suggest compensatory mechanisms immediately following an injury. We can use this study's results to guide future developments in stimulation-based therapy to alleviate the functional deficits from a stroke.

Introduction

Every 40 seconds, someone suffers from a stroke in the United States [1]. Of the 795,000 strokes that occur every year in the United States, around 87% are ischemic strokes. Stroke is the leading cause of long-term disability worldwide, especially in older patients [2]. An ischemic stroke occurs when blood flow to an area is blocked, leading to oxygen and nutrient deprivation in that area. A thrombus, also known as a blood clot, can cause such partial and full arterial blockages that lead to ischemia. Injuries, such as stroke, damage the neural network connections near and around the injury. These damages to the network lead to deficits in sensory functions like touch to motor functions like controlling arm movements. Current research shows that stimulation-based therapies can drive the reorganization of brain circuits to recover these impaired functions [3], establishing the importance of understanding the dynamics of neural circuits. Despite the prevalence of stroke, the neural network connectivity changes contributing to these functional deficits are not well understood.

Reviewing current models and experiment-based data on functional connectivity mechanisms and principles, specifically in the sensorimotor cortices, is essential for a thorough understanding of a network's response to injury such as stroke. The photothrombotic (PT) lesion technique has been used in rodent and non-human primate (NHP) models. The PT lesion technique induces ischemic lesions that are more like a natural stroke or traumatic injury than other lesion-inducing methods, such as aspiration induced ablation [4]. These similarities include both anatomical changes like axonal sprouting and electrophysiological changes like synchronous neural activity. One can measure these electrophysiological changes to understand the changes in functional connectivity during and after a lesion is induced [5]. The similarities between a natural stroke and a PT lesion are seen in tissue located around the lesion (perilesional tissue) and the hemisphere on the opposite side of the lesion (contralesional hemisphere). Compared to other techniques, the PT lesion better models a natural stroke.

Currently, the PT lesion technique is mostly implemented in rodent models and therefore is more studied than NHP models. A drawback to the rodent model is the maximum lesion size achieved [6]. Though some functional changes are observed in the cortex following the ischemic lesion, the resulting infarcts are small when scaled to a human brain's size by around three orders of magnitude. To better model a larger human brain, recording from a larger surface on the cortex, such as an NHP cortex, is needed. Recording electrophysiological data from a larger surface will allow for a better understanding of perilesional changes in network connectivity. Developmental learning and post-stroke recovery follow similar principles in functional connectivity changes and plasticity [7]. In one of a few clinical studies studying recovery post-stroke, the perilesional cortex affected recovery from post-traumatic injuries to the brain and central nervous system (CNS). Additionally, compensatory mechanisms were observed in the contralesional hemisphere [8]. Understanding these natural electrophysiological changes in unaffected cortical regions may lead to a more comprehensive preclinical model for stroke and post-stroke recovery.

Post-stroke recovery and early brain development stages can be similar in terms of the plasticity and functional connectivity mechanisms at work. In studying post-injury plasticity, it was observed that both spatial and temporal dynamics played a role in the recovery from injury [9]. Spatially, the perilesional tissue aided in blood flow recovery, while temporally, changes to the network aided in functional recovery. Within hours, changes in the brain's unaffected region, such as the contralesional hemisphere, were observed in response to changes in the ipsilesional cortex (hemisphere on the same side as the lesion) [10]. Though these compensatory mechanisms were observed, there was not as much information on the network changes as on the anatomical changes [11]. These network changes can be studied by observing different characteristics of local field potentials (LFPs). LFPs are recordings of electrical neural activity and are oscillatory by nature. Some groups of neurons can have “synchronous neuronal activity," as mentioned before [4]. This synchronous behavior of neurons links the electrophysiology to functional connectivity [12].

Coherence is one well-studied metric for quantifying this synchronization of neurons at a frequency. NHP models have shown that coherent oscillations are increased if the two groups are spatially nearby. In specific motor tasks, the functionally connected regions had higher levels of synchronized activity. Following results from NHP and clinical studies, the changes in coherence can be used as a measure for quantifying functional connectivity post-injury.

My capstone project is doing a quantitative analysis of the neurophysiological changes resulting from an ischemic lesion, like an ischemic stroke, in the sensorimotor cortex of NHPs. There are three separate segments of signal over which I have calculated and visualized the coherence over time: baseline, illumination (when the ischemic lesion is induced), and post-photo-thrombosis (PT) (after the lesion has been induced). Coherence provides information on how different areas of the brain are synced. By analyzing these two metrics, there will be a better understanding of an ischemic lesion's comprehensive effects in the sensorimotor cortex of NHPs. Understanding these effects can help develop stimulation-based therapies in the future that focus on functional recovery.

Development of Design Specifications

Data was first collected from the Nomad device records electrical signals at a sampling rate of 30,000 Hz. It was then down sampled to 1,000 Hz. The four frequency bands of interest were theta (4-7 Hz), beta (12-29 Hz), low gamma (30-59 Hz) and high gamma (60-150 Hz). To capture high gamma frequencies, the lowest sampling frequency would need to be 300 Hz. A sampling frequency of 1000 Hz satisfies this criterion. To analyze signal power, the low gamma band was used as it represents local neural activity well [13].

Many of the design constraints in this project are the parameter choices for mathematical functions like coherence, principal component analysis, and k-means clustering. Since coherence is the ratio of cross spectral density between two signals and the auto-spectral density of each individual signal, it requires similar parameters to a Fourier transform. As mentioned previously, the sampling frequency was 1000 Hz. Each value for coherence represents the pair-wise coherence at a given frequency for a partition of a signal segment. The signal segment in our case was 30 minutes to capture overall changes more easily from the baseline, illumination and post-PT segments. Each 30-minute segment was further split into 20-second partitions, or a sample size of 20,000. There was also an overlap of 10 seconds for each partition. As with any Fourier transform, a window is needed to mitigate effects from any discontinuities at the boundary of each partition. A Hamming window is a common option for frequency-based analysis of neural signals.

An exploratory data analysis project on NHP neurophysiology brings up several ethical and societal considerations. This project is critical for preclinical studies that can address the current gap between rodent and human studies, such as in physiological differences [14]. In the United States, primate research for neurological disorders is supported by the NIH and BRAIN Initiative; however, it is controversial and heavily regulated research [15]. The NERD Lab is part of the Washington National Primate Research Center (WaNPRC). As such, when any work is done with NHPs, like recording field potentials from an NHP cortex, all protocols, guidelines, and requirements are approved by the UW Institutional Animal Care and Use Committee (IACUC). All procedures for collecting the data for this project were approved by IACUC.

Design Specification	Value
Sampling Frequency of LFP	>300 Hz
Coherence – partition size	20 seconds (20,000 samples)
Coherence – overlap size	10 seconds (10,000 samples)
Coherence – window	Hamming

Table 1. Summary of Design Specifications

Materials and Methods

The data for this project was collected from two adult male rhesus macaques (Monkey D and Monkey E) using the photothrombotic (PT) stroke technique implemented in the NERD Lab, rather than in rodents as mentioned previously. When this technique is used in NHPs, it serves as a good preclinical model for stroke and other neurological disorders due to the similarities between NHP and human brains. A craniotomy was performed on both hemispheres of each monkey covering the primary somatosensory (S1) cortex. Next, a durotomy replaced the natural dura with a transparent artificial dura to allow for optical access to the cortical surface. An advantage of the PT stroke technique is the ability to precisely control the size and location of the ischemic lesion[16]. This precision was accomplished using an opaque silicon mask fitted over the artificial dura and containing gaps with pre-determined sizes to control light exposure (Figure 1a). Rose-bengal, a photoactive dye, was infused intravenously. Photoactivation of the dye triggers the release of reactive oxygen species (Figure 1b). This leads to platelet activation and aggregation at the site and eventually results in thrombosis, effectively inducing an ischemic lesion. In Monkey D, the left hemisphere was illuminated, and is the ipsilesional hemisphere. In Monkey E, the right hemisphere was illuminated and is the ipsilesional hemisphere.

Figure 1. Schematic of photothrombotic stroke technique. A) Mask with pre-determined aperture fitted over an artificial dura over the cortex following a craniotomy and durotomy. B) Illumination of cortical surface through silicon mask.

Electrophysiological data was collected using an electrocorticographic (ECoG) array laid on the surface of S1 (Figure 2). The custom designed μECoG array was made of a transparent polymer embedded with 32 flexible platinum electrodes. This recording setup gave our lab the unique capability to record neural data on a large-scale covering about 5 cm^2 of cortex.

Figure 2. Image of custom-designed electrocorticography (ECoG) array.

The recording sampling rate was 30,000 Hz. The electrophysiological recording was segmented into three parts. The first was a baseline recording, lasting about 30 minutes. Next was the illumination, also lasting about 30 minutes, which is when the Rose-bengal dye was activated. Finally, there was a post-PT recording, lasting around 3 hours, which captured electrophysiological activity as the ischemic lesion progressed. In addition to electrophysiological recording, optical coherence tomography angiography (OCTA) images were captured during the baseline period and three hours post-PT (Figure 3). These images were captured using a swept-source OCT system. These images were used to assess changes to the local microvasculature before and after the lesion was induced.

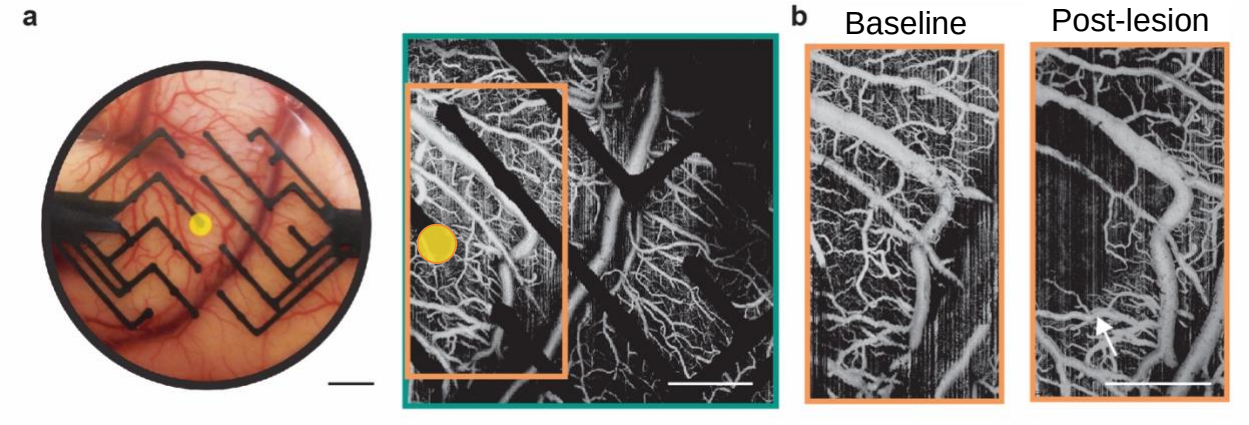

Figure 3. Optical coherence tomography angiography images for Monkey D. A) Image of ECoG array laid on the cortical surface (lesion location highlighted in yellow) and baseline OCTA image with electrode array. B) Baseline and post-lesion OCTA images for a zoomed in region boxed in orange.

Signal power analysis was completed using MATLAB and Python. The raw signal from the Nomad was down sampled to 1000 Hz and cleaned to remove any artifact. It was also notch filtered to at multiples of 60 Hz to remove any fixed-frequency noise from power lines during recording. The signal was then filtered into the low gamma band (30-59 Hz). To verify that any changes of power were the result of the photothrombotic lesion rather than naturally occurring transient changes on the cortex, the change in variance in power in baseline and in post-PT.

Data analysis for coherence was completed using Python (SciPy, NumPy, and scikit-learn) and MATLAB. For statistical analysis, tests like a paired t-test were used to detect any significant changes between groups. Before coherence was calculated the raw signal was down sampled to 1000 Hz, cleaned to remove any artifact, and filtered into theta (4-7 Hz), beta (12-29 Hz), low gamma (30-59 Hz), and high gamma (60-150 Hz) frequency bands. Coherence is formulated as

$$C_{xy}(f) = \frac{|G_{xy}(f)|^2}{G_{xx}(f)G_{yy}(f)}$$

The term $C_{xy}(f)$ is the cross-spectral density between signals x(t) and y(t), in this case signals from two electrodes, and $C_{xx}(f)$ and $C_{yy}(f)$ are the auto-spectral densities for x and y. A coherence of 1 indicates a high relation between two signals, and a coherence of 0 indicates no relation. Coherence was calculated for each minute of the cleaned and filtered signal. Within each one-minute segment of signal, coherence was calculated in 20 second windows, with a 10 second overlap between windows, for each pair of electrodes. For Monkey D, electrode 8 was excluded from analysis. For Monkey E, electrodes 8, 24, and 25 were excluded from analysis. These electrodes were excluded because of the high amounts of artifact and noise throughout the recording period.

Statistical analysis was completed using Python and MATLAB. For comparisons between baseline and post-PT power and coherence, a paired t-test was used. The generated p-values were also compared to a family-wise error rate to account for multiple comparisons.

Results

Ipsilesional Power

The difference in low-gamma band signal power for the first 30 minutes of baseline segment and last 30 minutes of post-lesion segment was calculated first (Figure 4). These differences highlighted a region near where the lesion was induced where there was a significant decrease in power. In addition, there were some electrodes with no change in power and an increase in power. To better separate these three groups, k-means clustering was performed to sort the electrodes. Following k-means clustering, three groups of electrodes were identified and could be characterized by their overall change in power (Figure 5).

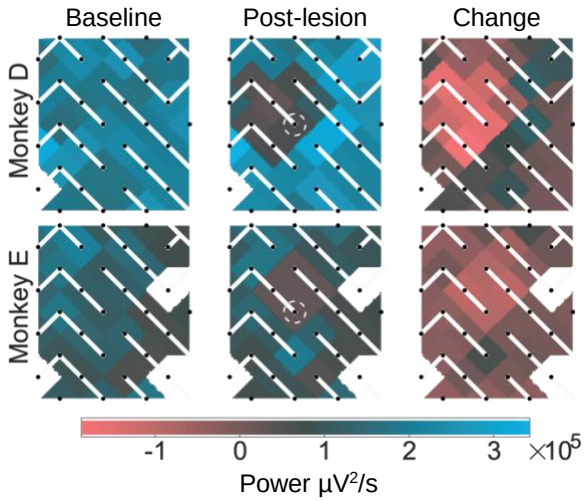

Figure 4. Changes in low gamma band signal power from baseline to post lesion. (From left to right) Average power for first 30 minutes of baseline, average power for last 30 minutes of post-lesion, difference between segments. Dotted circle in post-lesion heat map indicates illuminated area.

However, simply sorting the electrodes by their overall change in power from baseline to post-PT was a more intuitive way of clustering the electrodes. For each channel, the set of baseline power values (first 30 minutes) and set of post-lesion power values (last 30 minutes) were compared via a t-test. Electrodes were then sorted by their overall change, rather than using k-means clustering. The comparison between the two clusters is shown in in Figure 5.

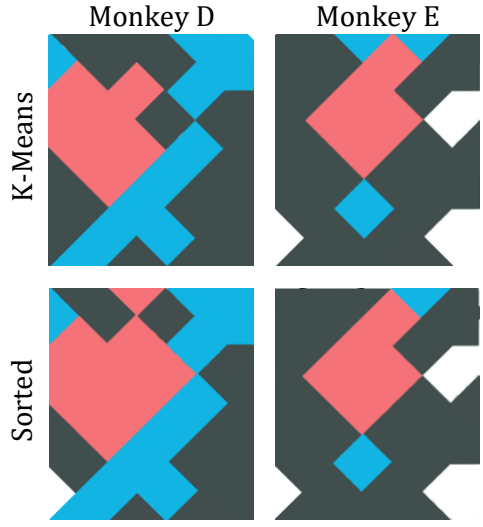

Figure 5. Iterations of electrode clustering through k-means clustering (first row) and sorted (second row) by changes in power.

In both cases, the region with an overall decrease in power coincided with the location of the photothrombotic stroke. There was also a minimal difference between the sorted clusters and k-means clusters. From this point on, the sorted clusters were used for further analysis. The cluster with an overall decrease in power was labelled as Cluster 1, the lesion cluster, denoted by pink. The cluster with no change in power was labelled as Cluster 2, denoted by grey. The cluster with an overall increase in power was labelled as Cluster 3, denoted by blue. Interestingly, the regions of

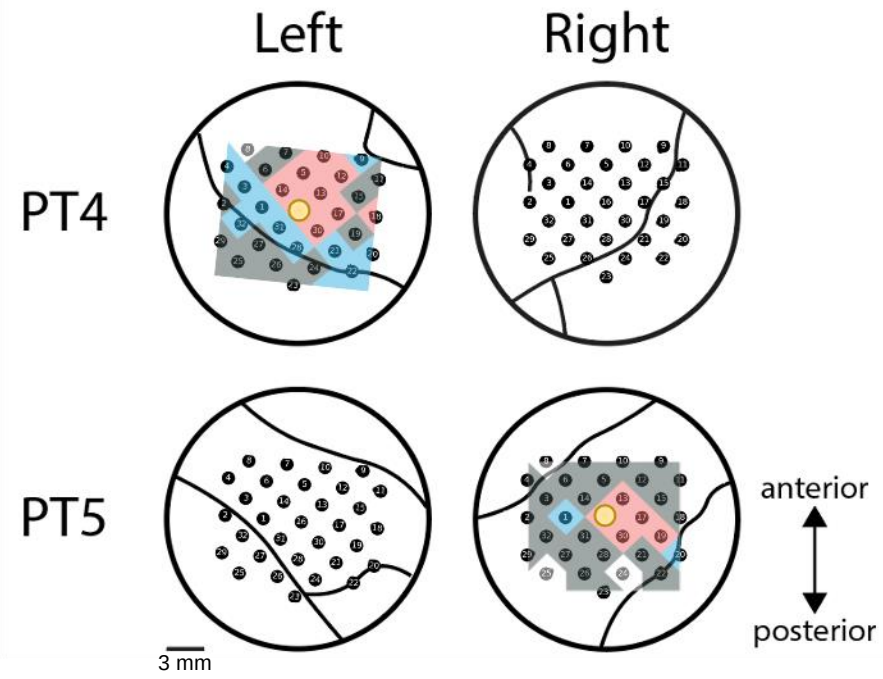

Figure 6. Second iteration of ipsilesional electrode clusters mapped onto the left (PT4 ipsilesional) and right (PT5 ipsilesional) hemispheres of the brain. The lesion location is highlighted in yellow.

increases in power in both Monkey D and Monkey E align with the central sulcus when an anatomical map is overlayed with the color-coded array (Figure 6). The central sulcus separates the somatosensory and motor cortices. By plotting power of each electrode over time, we were able to further demonstrates this separation in electrodes based on overall change in power from baseline to post-PT. During the illumination period, power decreases across all channels (Figure 7). Further, the cluster with an overall decrease in power has very low power relative to the other two clusters following the illumination period.

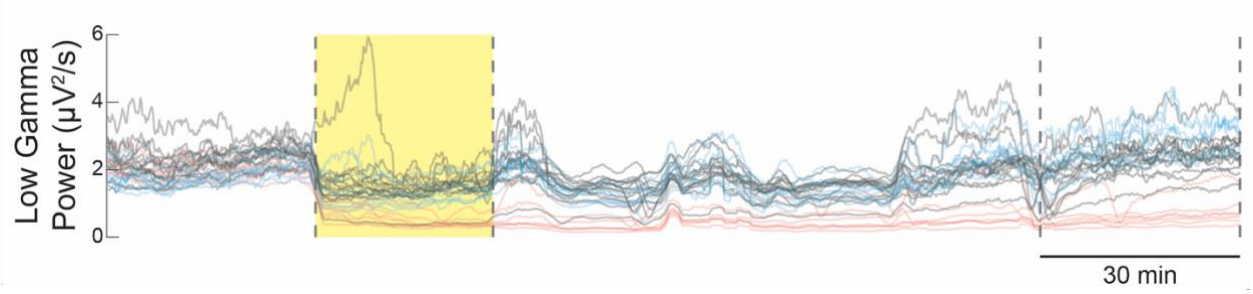

Figure 7. Power trace of electrodes over time, with clusters highlighted in respective colors (decreasing – pink, no change – grey, increase - blue. Illumination period highlighted in yellow.

Ipsilesional Coherence – Principal Component Analysis

Like the analysis for ipsilesional power, I also wanted to check if there were similar changes in coherence that would form clusters. The goal here was to find clusters independent of the power analysis. Once these clusters were found, it would be interesting to see how the clusters from power aligned with the clusters from coherence.

The first step in this analysis was to look at traces of the connection over time and observe if there were distinct clusters forming, as we saw in power analysis. However, accounting for every pair-wise connection in the electrode array, meant looking at about 1,024 connections per frequency band, per animal. As a result, I began to look at each electrode individually and visualizing each connection to a different electrode.

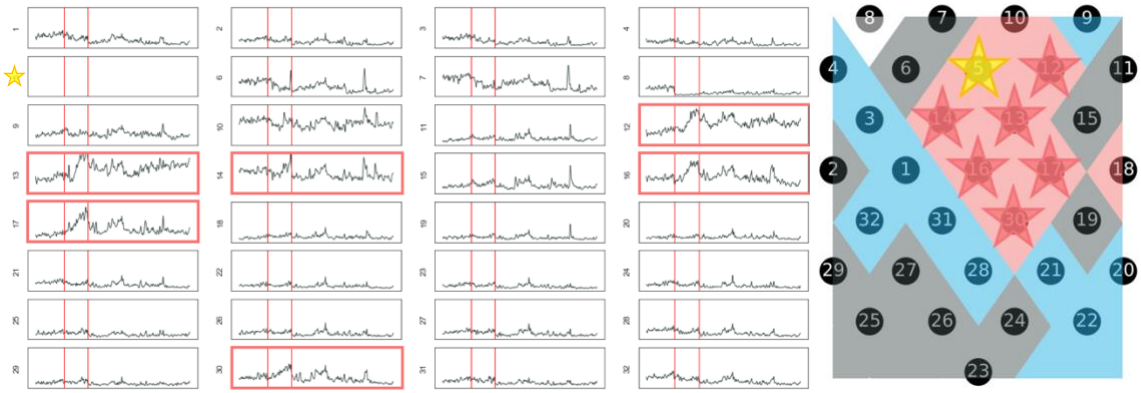

Figure 8. Coherence between Electrode 5 (yellow star) and rest of network for Monkey D over entire recording session (baseline, illumination and post-lesion period separated by vertical red lines). Plots on the left boxed in pink align with the pink stars on the right.

All connections were plotted excluding the connection of an electrode to itself, as this would always have a coherence of 1. As seen in Figure 8, there were some pair-wise connections that looked similar. When the locations of these electrodes were examined, it was evident that they aligned with the lesion cluster identified through power analysis.

There were two issues with this approach. This still depended on the power analysis to confirm similarities between groups. In addition, it would be time consuming and inefficient to examine each set of 32 plots for each electrode, each frequency band, and each animal. Rather than

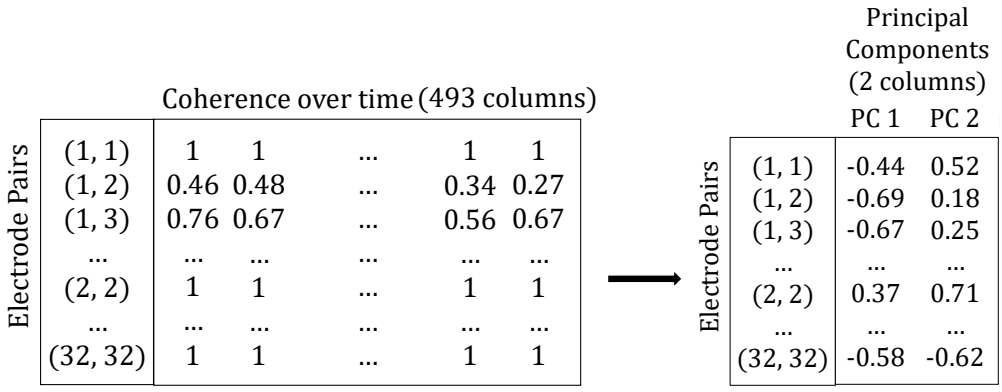

Figure 9. Schematic of transformation of 2D matrix to principal component space. The original columns, representing pair-wise coherence over time, are reduced to their principal components.

take the time to visually examine each electrode, I decided to do principal component analysis (PCA), a more objective method to identify potential clusters. Principal component analysis identifies the maximum variance of the data, in this case pair-wise coherence over time, and reduces the data into fewer dimensions, making it easier to interpret (Figure 9). In this project, the two-dimensional matrix of electrode pairs and time was reduced in the time dimensions to 2 principal components.

The principal component transformation transforms the data into a new coordinate system, where the new orthogonal axes are its principal components (PC). The first two PCs were used for this transformation. An important metric in principal component analysis is the explained variance (EV) ratio, which can be calculated for each PC. An EV ratio of 75% for example, means that 75% of the variance in the data can be attributed to that PC. The first PC is also the line of best fit, and will have the highest EV ratio, and the EV ratio will decrease for each subsequent PC.

PCA quantifies what the previous visualizations were showing. Electrodes that have similar changes over time will be near each other in the transformed PC space. Each point in the transformed space represents one pair of electrodes. As seen in Figure 10, there are no clusters with visible separation in the principal component space.

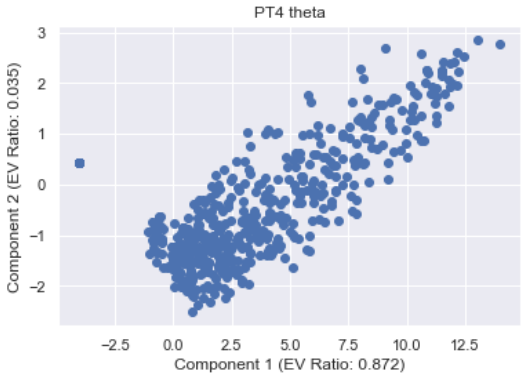

Figure 10. Transformed principal component space, reducing the time dimension.

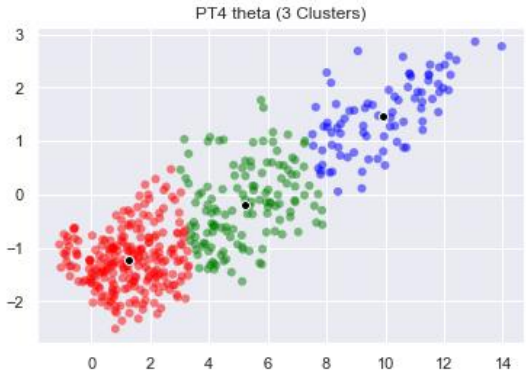

Figure 11. Transformed electrodes color coded after application of the k-means clustering algorithm.

The k-means clustering algorithm was then applied to the transformed array to determine which clusters (if any) were forming in the transformed space (Figure 11). However, there were no distinct clusters forming. After tracing the points from PC space back onto the network using an inverse transform, it was evident that many of the connections fell into one cluster and the clusters did not follow an anatomically intuitive pattern. This was the case for all frequency bands in both monkeys.

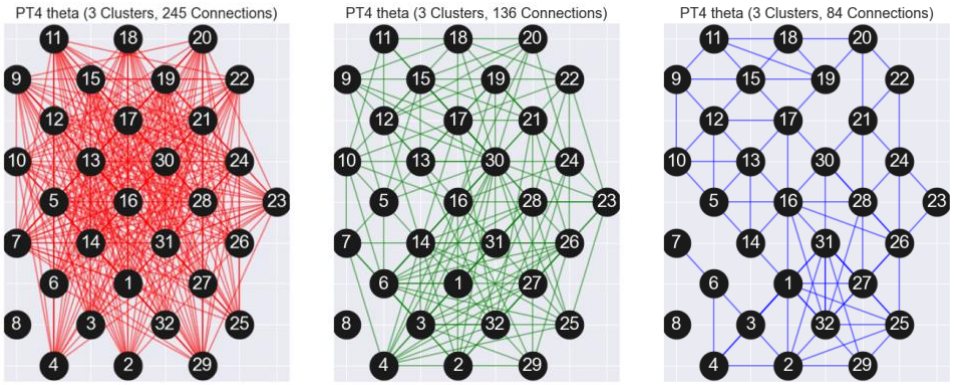

Figure 12. Example of clustered electrodes from PC space mapped back onto the network.

Using coherence alone, there were no identifiable clusters of pair-wise connections which could be mapped on to electrode array (Figure 12). The coherence analysis from this point on was by applying the three clusters found through power.

Ipsilesional Coherence Analysis

The ipsilesional coherence analysis can be split up into two main parts: the overall coherence change across the entire ipsilesional network and the coherence changes between different clusters as identified through low gamma band power. To first understand how the entire ipsilesional network changed in terms of coherence, the average coherence for the first 30 minutes of baseline and last 30 minutes of post-lesion were calculated. A paired t-test was done to compare the average coherence for baseline to the average coherence for the last 30 minutes of post-lesion, at 60-second intervals. A family wise error rate (FWER) of 0.00125 was used to account for multiple comparisons.

For ipsilesional network-wide coherence, coherence in the theta band decreased from 0.409 to 0.312 ($p = 1.17e-178$) for Monkey D and 0.483 to 0.433 ($p = 3.17e-30$) for Monkey E (Figure 13). Coherence in the beta band, decreased in Monkey D ($p = 2.54e-87$) but a significant increase in Monkey E ($p = 8.02e-183$). In Monkey E, coherence in the low gamma band increased from 0.138 to 0.245 ($p = 5.98e-223$) and increased in the high gamma band from 0.112 to 0.179 ($p = 1.35e-226$). Coherence changes in Monkey D were not significant.

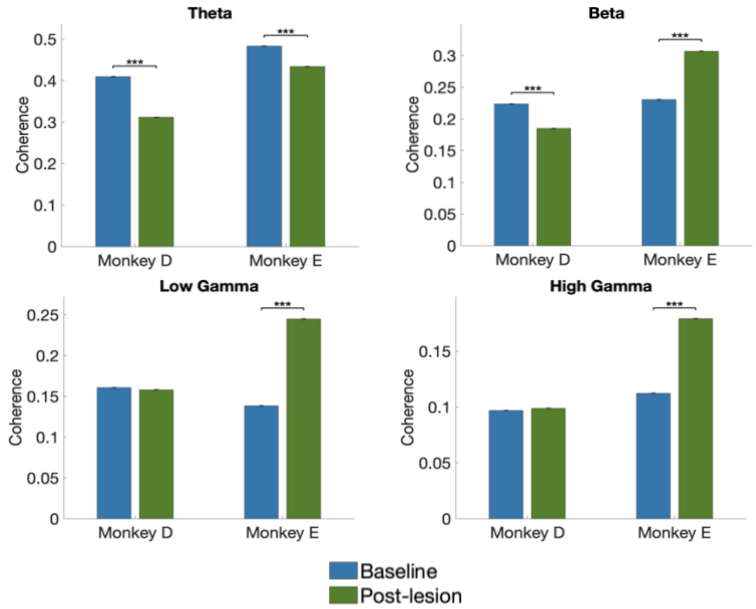

Figure 13. Average coherence for first 30 minutes of baseline and last 30 minutes of post-lesion for each frequency band (theta, beta, low gamma, high gamma).

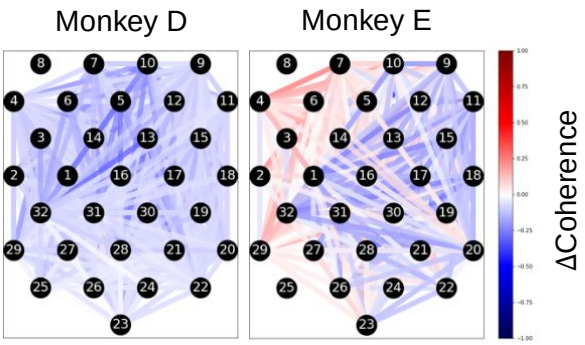

Figure 14. Change in theta-band coherence from first 30 minutes of baseline and last 30 minutes of post-lesion for each pair of electrodes.

These changes can also be visualized on a pair-by-pair level, as seen in Figure 14, for the theta band. Increases are color coded by red, while decreases are color coded by blue. The change for a pair-wise connection lies between -1 and +1, with larger changes indicated by darker colors. The network visualization shows finer detail about the ipsilesional network. In the top left corner of Monkey E's ipsilesional network, there is a region with an increase in coherence, though the overall change in coherence is negative. In Monkey D, there is a region in the upper middle with a decrease of a larger magnitude.

The next part of ipsilesional coherence analysis was looking at coherence and grouping electrodes based on their overall power change. To summarize from the previous section, there were three clusters found through low-gamma signal power: overall decrease (which included the lesion for both monkeys), no change, and increase. Two new terms will be defined to better differentiate the analysis. Intra-lesion will refer to the coherence of the electrodes in the lesion cluster with itself. Interlesion will refer to the coherence of the electrodes in the lesion cluster with the rest of the network. The same alpha value was used for intra-lesion and inter-lesion analysis as network-wide coherence.

For intra-lesion coherence, coherence in the theta band decreased from 0.583 to 0.495 ($p = 3.31e-9$) for Monkey D and 0.808 to 0.722 ($p = 0.003$) for Monkey E (Figure X). Coherence in the beta band, increased in Monkey E ($p = 8.41e-7$), but there was no significant change in Monkey D. Coherence in the low gamma band increased from 0.257 to 0.317 ($p = 1.63e-8$) for Monkey D and 0.808 to 0.722 ($p = 1.56e-9$) for Monkey E. Coherence in the high gamma band also increased from 0.172 to 0.212 ($p = 8.38e-11$) for Monkey D and 0.277 to 0.410 ($p = 9.36e-7$) for Monkey E.

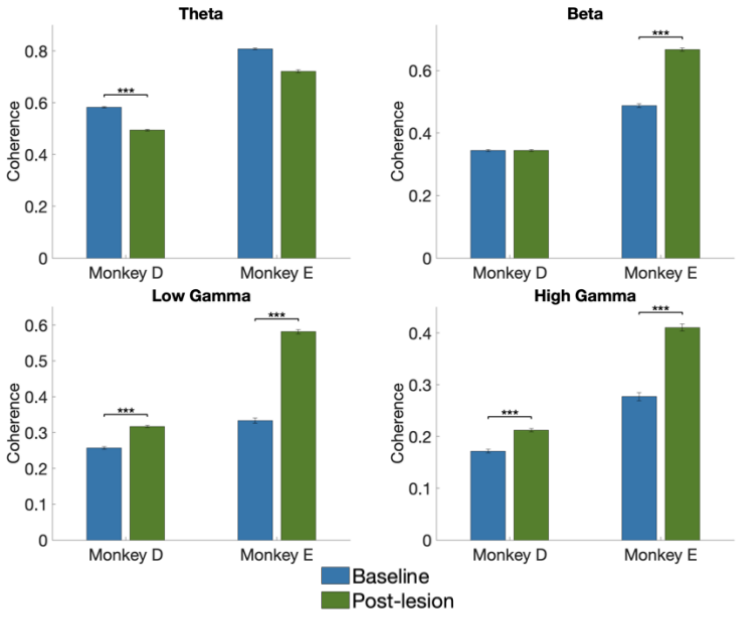

Figure 15. Average intra lesion coherence of for first 30 minutes of baseline and last 30 minutes of post-lesion for each frequency band (theta, beta, low gamma, high gamma).

The lack of significance in the theta band for Monkey E could be attributed to the fewer number of electrodes in the lesion cluster. In Monkey D, there were nine electrodes in the lesion cluster, while in Monkey E, there were only five. Unlike in the overall changes in low and high gamma coherence, the increases in both monkeys are significant when focusing on the cluster with an overall decrease in power and contains the lesion.

These changes in low gamma (Figure 16) and high gamma (Figure 17) can also be visualized as a network. As mentioned previously, there are fewer electrodes in the cluster closest to the lesion

for Monkey E. When looking at the lesion cluster, pair-wise coherence increases for every connection. In Monkey D, pair-wise coherence increases for all but one pair of electrodes (E30 and E12). Overall, in intra-lesion coherence, there is a decrease in the theta band and an increase in the low and high gamma bands 3 hours after an ischemic lesion has been induced.

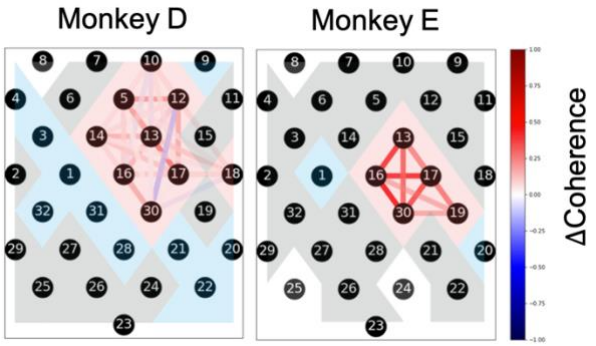

Figure 16. Change in low gamma-band coherence from first 30 minutes of baseline and last 30 minutes of post-lesion for each pair of electrodes.

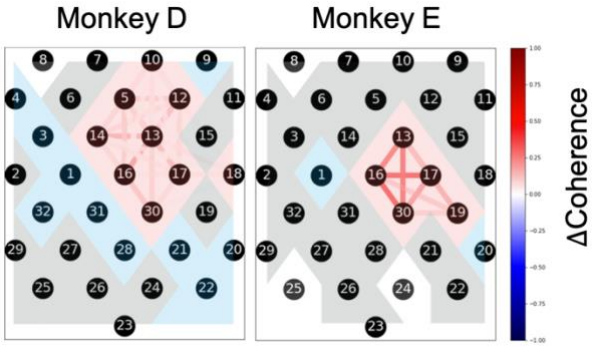

Figure 17. Change in high gamma-band coherence from first 30 minutes of baseline and last 30 minutes of post-lesion for each pair of electrodes.

For intra-lesion coherence, coherence in the theta band decreased from 0.380 to 0.252 (p = 1.93e-41) for Monkey D and 0.528 to 0.420 (p = 2.69e-14) for Monkey E (Figure 18). Coherence in the beta band decreased from 0.184 to 0.141 (p = 2.08e-22) for Monkey D and increased from 0.219 to 0.322 (p = 2.69e-14) for Monkey E (p = 3.51e-22). Coherence in the low gamma band increased from 0.119 to 0.123 (p = 0.135) for Monkey D and 0.105 to 0.245 (p = 6.07e-41) for Monkey E. Coherence in the high gamma band also increased from 0.058 to 0.062 (p = 0.011) for Monkey D and 0.076 to 0.157 (p = 1.77e-44) for Monkey E.

In the overall network, however, there was a decrease in low gamma coherence in Monkey D. This is the result of a decrease in low gamma coherence between the no-change and increase in power clusters. Coherence decreased between these two clusters from 0.139 to 0.119 (p = 1.57e-20). The connection between these two clusters is not considered in inter-lesion coherence, resulting in an overall increase.

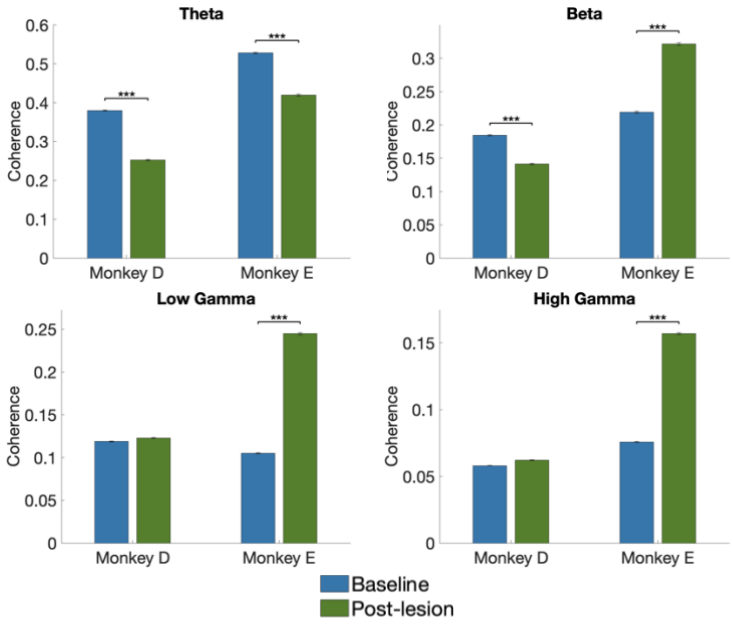

Figure 18. Average inter-lesion coherence of for first 30 minutes of baseline and last 30 minutes of post-lesion for each frequency band (theta, beta, low gamma, high gamma).

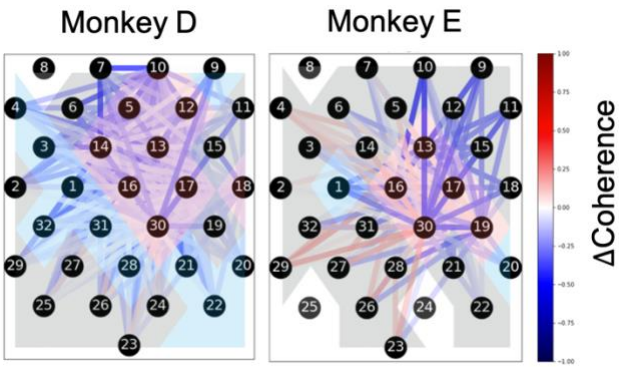

Figure 19. Change in theta-band inter-lesion coherence from first 30 minutes of baseline and last 30 minutes of post-lesion for each pair of electrodes.

The changes in the theta band inter-lesion coherence can also be visualized as the network (Figure 19). In Monkey D, most of the connections between the lesion cluster and the rest of the network are decreasing in coherence three hours post-lesion. In Monkey E, however, the right side of the ipsilesional network is decreasing while the left side of the network is increasing. Overall, in inter-lesion coherence, there is a decrease in the theta band and an increase in the low and high gamma bands 3 hours after an ischemic lesion has been induced.

Contralesional Power

Power analysis was also done on the contralesional hemisphere following the same method as ipsilesional power. Each electrode was sorted based on its overall change in power from the first 30 minutes of baseline to the last 30 minutes of the post-lesion segment. In both monkeys, there were no clusters with overall decreases in power, and as a result there were only two clusters (Figure 20).

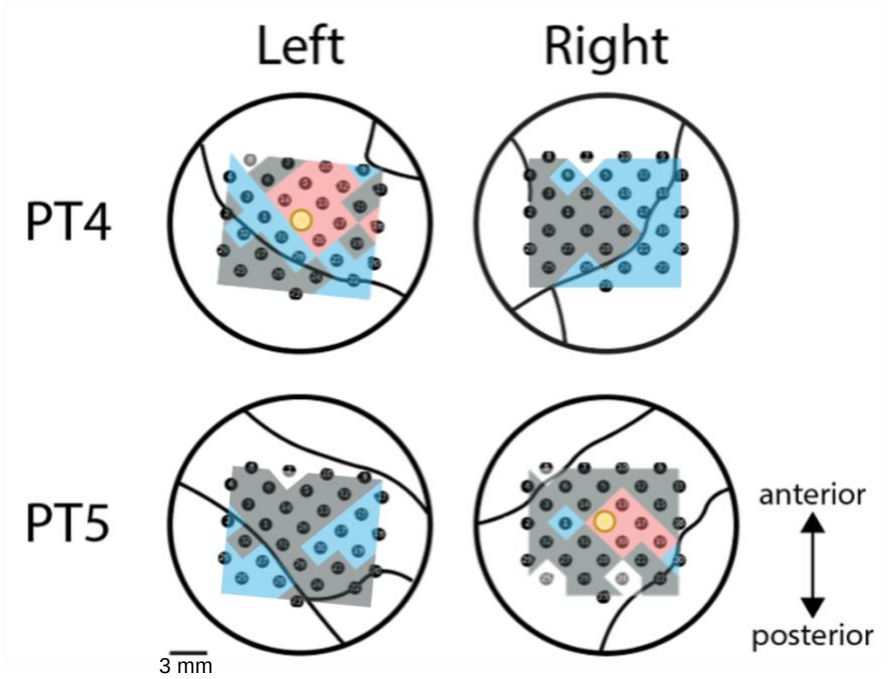

Figure 20. Contralesional electrode clusters mapped onto the right (PT4 contralesional) and left (PT5 contralesional) hemispheres of the brain. The lesion location is highlighted in yellow.

Contralesional Coherence

Coherence was also calculated on the contralesional hemisphere. The contralesional hemisphere is the hemisphere opposite the side where the lesion was induced. Like ipsilesional coherence, a paired t-test was done to compare baseline coherence to post-lesion coherence. The family wise error rate (FWER) was adjusted by setting α = 0.00625 to account for multiple comparisons.

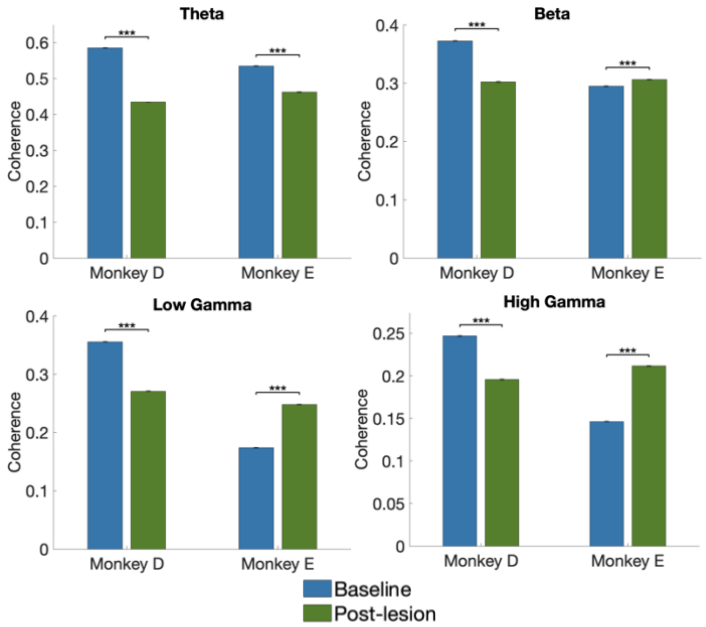

Figure 21. Average contralesional coherence for first 30 minutes of baseline and last 30 minutes of post-lesion for each frequency band (theta, beta, low gamma, high gamma).

For intra-lesion coherence, coherence in the theta band decreased from 0.585 to 0.434 (p = 5.24e-249) for Monkey D and 0.535 to 0.426 (p = 4.81e-66) for Monkey E (Figure 21). For all remaining bands, changes in coherence were not consistent across both Monkey D and Monkey E. For Monkey D, there was a significant decrease in beta (p = 8.70e-131), low gamma (p = 2.72e-177), and high gamma (p = 7.54e-118) coherence. For Monkey E, there was a significant decrease in beta (1.66e-06), low gamma (p = 3.69e-165), and high gamma (p = 1.81e-229) coherence.

In the network maps, most connections are decreasing for Monkey D (Figure 22). The connections on the left side of the array decreased with a larger magnitude (darker blue) than the right side of the array (lighter blue). Comparing these changes to the clusters found through signal power, the left side of the array was in the overall no change cluster. The right side of the array corresponded to an overall increase in power. In Monkey E, most connections in the upper right-hand side of the array are increasing. Connections closer to the bottom of the array are decreasing.

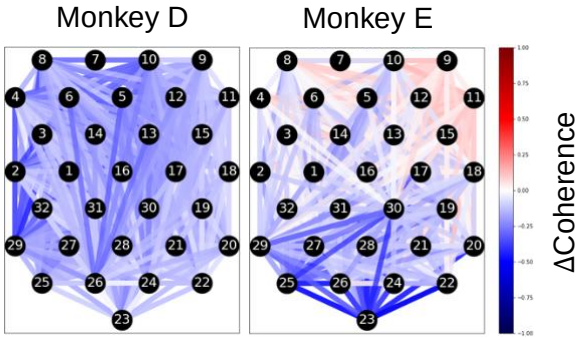

Figure 22. Change in theta-band coherence in the contralesional hemisphere from first 30 minutes of baseline and last 30 minutes of post-lesion for each pair of electrodes.

Cross Hemisphere Coherence

Finally, coherence between the ipsilesional and contralesional hemispheres was calculated. A paired t-test was done to compare baseline to post-lesion coherence. The family wise error rate (FWER) was adjusted by setting α = 0.0015625 to account for multiple comparisons.

Changes in cross-hemisphere coherence were only consistent in the theta band (Figure 23). In both Monkey D, coherence decreased from 0.176 to 0.155 (p = 2.37e-19) and from 0.248 to 0.212 (p = 2.75e-33) in Monkey E. For the remaining three bands, the changes in coherence from baseline to post-lesion were not consistent for both monkeys.

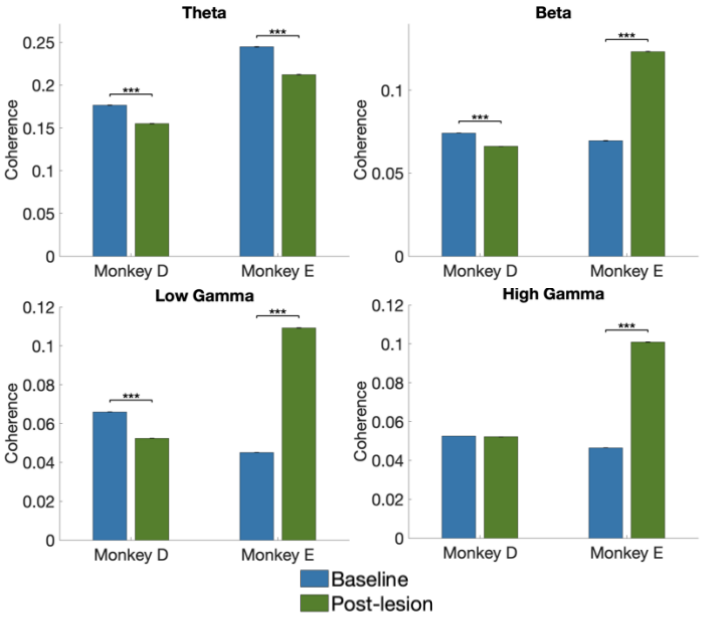

Figure 23. Average coherence across ipsilesional and contralesional hemispheres for first 30 minutes of baseline and last 30 minutes of post-lesion for each frequency band (theta, beta, low gamma, high gamma).

These changes can also be visualized as a network (Figure 24). In Monkey D, the ipsilesional hemisphere is the left array while in Monkey E, the ipsilesional hemisphere is the right array. Like the coherence for each individual hemisphere, the coherence for most connections in both hemispheres are decreasing for Monkey D from 0.176 to 0.155. For Monkey E, theta band coherence also aligns with results from each individual hemisphere. On the ipsilesional side, connections in the upper left region of the array increased. On the contralesional side, connections in the upper right region of the array also increased.

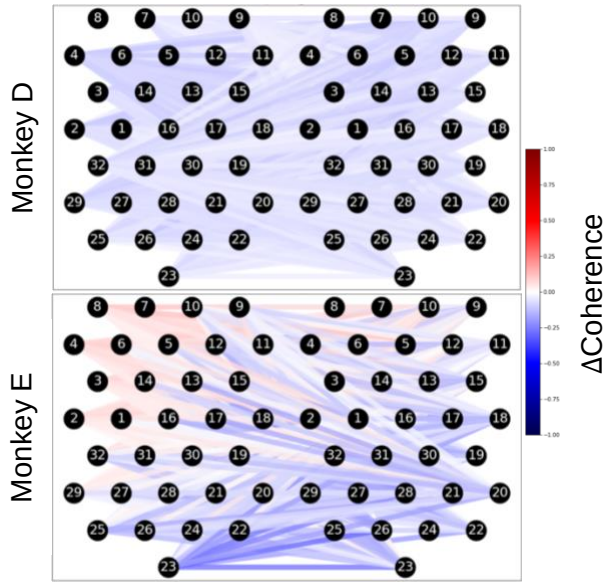

Figure 24. Change in theta-band coherence between the ipsilesional and contralesional hemispheres from first 30 minutes of baseline and last 30 minutes of post-lesion for each pair of electrodes.

Discussion

The results of the neurophysiological changes show that at the site of the photothrombotic lesion, there is a decrease in LFP signal low-gamma power three hours post-illumination. On the ipsilesional hemisphere, there are also regions of increases in power and no changes in power. The contralesional hemisphere only had regions with increases or no changes in power. These changes in power are what one would expect. After the lesion is induced and thrombosis occurs, neurons in the perilesional region are damaged, resulting in the decrease in power. On the contralesional hemisphere, there are no regions with decreases in power.

We also explored various changes in network connectivity using coherence as a metric. In addition to observing network-wide changes, we applied clusters found through power changes to connectivity. Two terms were defined to categorize these power-based connectivity changes: intralesion and interlesion. Across all analyses, there were decreases in the theta band coherence three hours following the induction of the photothrombotic lesion. The theta band falls into the 4-7 Hz range. Oscillations in the theta band could be the result of neurons that have a slower firing rate, typically excitatory neurons [13]. The decreases seen in the theta band suggest that there is decreased communication between excitatory neurons across the sensorimotor cortex. The decreases seen in contralesional coherence and cross hemisphere coherence also suggest that this decreased communication extends past the perilesional region and affects healthy neurons much further away from the lesion. Previous studies in rodents also support this decrease in excitability post-stroke [17, 18]. It has been observed that tonic gamma-aminobutyric acid (GABA) current increases following a stroke. Since GABA is an inhibitory neurotransmitter, increases in its current lead to a phase of hypo-excitability in the cortex post-stroke [18]. These findings align with the decrease in theta coherence observed in this project.

Further, ipsilesional analysis showed increases in low gamma and high gamma, especially when focused on the region where the lesion was induced. It was interesting and unexpected to see that though there was an overall expected decrease in power near the lesion, there was actually more connectivity within that region. Oscillations in the low and high gamma bands could be the result of inhibitory neurons, which are associated with faster spiking [19]. This suggests that while the activity of neurons at the site of the lesion is of a smaller magnitude, the activity is more in sync. In one rodent study, the largest frequency component from electrophysiology recordings increased from 15 Hz to 129 Hz in animals with a photothrombotic lesion, supporting the observed increase in higher frequency communication in the peri-lesion area [20]. In addition to the hypo-excitability, the increases in high frequency connectivity suggests the peri-lesion region is in a hyper-inhibition phase three hours following the induction of a lesion. This can also be some kind of compensatory mechanism for the damage occurring at the site of the lesion. To compensate for the loss of neurons and communication in the future, inhibitory neurons surrounding lesion may increase their activity and allow for some reorganization. This reorganization has been observed in squirrel monkeys through anatomical analysis [21]. Overall, the changes in connectivity suggest that there is both hypo-excitability and hyper-inhibition occurring immediately following the induction of a focal ischemic lesion. This could be to compensate for the death of nearby neurons and resulting loss of communication from the lesioned area.

There are some similarities between results of this project and previous studies in neurophysiology and neurotransmitters. However, there are also some pieces of conflicting evidence between studies, most likely due to the differences in the animal studied and the amount of time that had passed between the induction of the lesion and the observations. For example, one study looked at functional connectivity (using cross correlation as a metric) 9 and 23 days following a unilateral photothrombotic lesion in rodents [22]. Nine days post-lesion, there was a decrease in the gamma band connectivity. It is possible that the connectivity in the gamma band increases at first, and then decreases as the stroke continues to impact the tissue. The stroke toolbox developed in the NERD

Lab allows us to measure these kinds of changes immediately after a cortical lesion is induced, unlike many other setups which record several days or weeks after lesion induction.

There are several avenues for future work. Using the current data, we could also look at delta-band coherence, as there are several studies that have used this frequency for analyzing functional connectivity. Decreases have been observed in delta band functional connectivity 9 days post-lesion and decreases in spike-field coherence have been observed in low frequency oscillations (1.4-5 Hz) 5 days post-stroke [22]. Lower frequencies have been associated as a neurophysiological marker for motor control post-stroke [23]. Understanding the mechanisms behind changes in lower frequencies than theta could be important for stroke recovery, specifically stroke in the sensorimotor cortices. To improve confidence in similarities to previous studies, the recording period can be lengthened past three hours or multiple recording can be done over several days. Finally, behavioral studies can be incorporated into the electrophysiological recordings to further understand the short-term impacts of a lesion on sensory and motor function.

As stated initially, there is a biomedical need to understand that electrophysiological changes in NHPs immediately following the induction of an ischemic lesion. Many previous studies either focus on changes on the order of weeks or days or have been done in rodent models. This project is one of the few NHP studies exploring the immediate change in electrophysiology following an ischemic lesion. Though this project alone is far from having a direct clinical impact, it increases knowledge at the pre-clinical stage. By understanding the cortical network's natural response to injury like an ischemic lesion, we can be one step closer to using stimulation to counteract those changes and recover functional connectivity. As past research in the lab and field suggests, there is great potential to use stimulation to modulate the network and develop a therapy for stroke [3]. Knowledge of the electrophysiological effects of ischemia on the cortex of an NHP is essential to taking this next step of using stimulation to rewire neural circuits around the injury towards functional recovery.

Acknowledgements

This capstone and the research behind it would not have been possible without the endless support by members of the NERD Lab, especially my advisor Dr. Azadeh Yazdan-Shahmorad and graduate mentor Karam Khateeb. I would also like to thank Dr. Paul Yager, Dr. Chris Neils, and Dr. Alyssa Taylor for their guidance in the capstone classes and students in the BIOEN 402 track (Jacelyn Bain, Abigail Colmenares, Aleah DeSchmidt, Karina LaValley, Nadia Siddiqui, and Marly Koala) for their help with revisions on this report. Finally, I would like to thank both the Mary Gates Fellowship and Washington Research Foundation (WRF) Innovation Undergraduate Fellowship in Neuroengineering through the UW Institute for Neuroengineering (UWIN) for their financial assistance for this project over the past year.

References

[1] M. Katan and A. Luft, "Global Burden of Stroke," no. 1098-9021 (Electronic).

[2] M. J. Benjamin Ej Fau - Blaha *et al.*, "Heart Disease and Stroke Statistics-2017 Update: A Report From the American Heart Association," no. 1524-4539 (Electronic).

[3] A. Yazdan-Shahmorad, D. B. Silversmith, V. Kharazia, and P. N. Sabes, "Targeted cortical reorganization using optogenetics in non-human primates," (in eng), *Elife,* vol. 7, 05 2018, doi: 10.7554/eLife.31034.

[4] S. T. Carmichael and M.-F. Chesselet, "Synchronous Neuronal Activity Is a Signal for Axonal Sprouting after Cortical Lesions in the Adult," *The Journal of Neuroscience,* vol. 22, no. 14, pp. 6062-6070, 2002, doi: 10.1523/jneurosci.22-14-06062.2002.

[5] A. N. Clarkson, H. E. López-Valdés, J. J. Overman, A. C. Charles, K. Brennan, and S. T. Carmichael, "Multimodal Examination of Structural and Functional Remapping in the Mouse Photothrombotic Stroke Model," *Journal of Cerebral Blood Flow & Metabolism,* vol. 33, no. 5, pp. 716-723, 2013, doi: 10.1038/jcbfm.2013.7.

[6] T. C. Harrison, G. Silasi, J. D. Boyd, and T. H. Murphy, "Displacement of Sensory Maps and Disorganization of Motor Cortex After Targeted Stroke in Mice," *Stroke,* vol. 44, no. 8, pp. 2300-2306, 2013, doi: doi:10.1161/STROKEAHA.113.001272.

[7] R. Teasell, N. A. Bayona, and J. Bitensky, "Plasticity and Reorganization of the Brain Post Stroke," *Topics in Stroke Rehabilitation,* vol. 12, no. 3, pp. 11-26, 2005.

[8] T. Schallert, S. M. Fleming, and M. T. Woodlee, "Should the injured and intact hemispheres be treated differently during the early phases of physical restorative therapy in experimental stroke or parkinsonism?," (in eng), *Phys Med Rehabil Clin N Am,* vol. 14, no. 1 Suppl, pp. S27-46, Feb 2003, doi: 10.1016/s1047-9651(02)00055-4.

[9] A. Sigler and T. H. Murphy, "In Vivo 2-Photon Imaging of Fine Structure in the Rodent Brain," *Stroke,* vol. 41, no. 10_suppl_1, pp. S117-S123, 2010, doi: doi:10.1161/STROKEAHA.110.594648.

[10] M. H. Mohajerani, K. Aminoltejari, and T. H. Murphy, "Targeted mini-strokes produce changes in interhemispheric sensory signal processing that are indicative of disinhibition within minutes," *Proceedings of the National Academy of Sciences,* vol. 108, no. 22, pp. E183-E191, 2011, doi: 10.1073/pnas.1101914108.

[11] S. C. Cramer, "Stroke recovery: how the computer reprograms itself. Neuronal plasticity: the key to stroke recovery. Kananskis, Alberta, Canada, 19-22 March 2000," in *Mol Med Today*, vol. 6, no. 8). England, 2000, pp. 301-3.

[12] V. N. Murthy and E. E. Fetz, "Coherent 25- to 35-Hz oscillations in the sensorimotor cortex of awake behaving monkeys," *Proceedings of the National Academy of Sciences of the United States of America,* vol. 89, no. 12, pp. 5670-5674, 1992.

[13] G. Buzsáki, C. A. Anastassiou, and C. Koch, "The origin of extracellular fields and currents--EEG, ECoG, LFP and spikes," (in eng), *Nat Rev Neurosci,* vol. 13, no. 6, pp. 407-20, May 2012, doi: 10.1038/nrn3241.

[14] D. H. Freedman. (1992) New Theory on How The Aggressive Egg Attracts Sperm. *Discover*.

[15] N. I. o. Health, "The Brain Initiative," ed.

[16] D. J. Cook and M. Tymianski, "Nonhuman primate models of stroke for translational neuroprotection research," (in eng), *Neurotherapeutics,* vol. 9, no. 2, pp. 371-9, Apr 2012, doi: 10.1007/s13311-012-0115-z.

[17] P. Bartolomeo and M. Thiebaut de Schotten, "Let thy left brain know what thy right brain doeth: Inter-hemispheric compensation of functional deficits after brain damage," (in eng), *Neuropsychologia,* vol. 93, no. Pt B, pp. 407-412, Dec 2016, doi: 10.1016/j.neuropsychologia.2016.06.016.

[18] S. T. Carmichael, "Brain excitability in stroke: the yin and yang of stroke progression," (in eng), *Arch Neurol,* vol. 69, no. 2, pp. 161-7, Feb 2012, doi: 10.1001/archneurol.2011.1175.

[19] J. A. Cardin *et al.*, "Driving fast-spiking cells induces gamma rhythm and controls sensory responses," (in eng), *Nature,* vol. 459, no. 7247, pp. 663-7, Jun 2009, doi: 10.1038/nature08002.
[20] K. Schiene *et al.*, "Neuronal hyperexcitability and reduction of GABAA-receptor expression in the surround of cerebral photothrombosis," (in eng), *J Cereb Blood Flow Metab,* vol. 16, no. 5, pp. 906-14, Sep 1996, doi: 10.1097/00004647-199609000-00014.
[21] N. Dancause, "Vicarious function of remote cortex following stroke: recent evidence from human and animal studies," (in eng), *Neuroscientist,* vol. 12, no. 6, pp. 489-99, Dec 2006, doi: 10.1177/1073858406292782.
[22] F. Vallone *et al.*, "Post-Stroke Longitudinal Alterations of Inter-Hemispheric Correlation and Hemispheric Dominance in Mouse Pre-Motor Cortex," (in eng), *PLoS One,* vol. 11, no. 1, p. e0146858, 2016, doi: 10.1371/journal.pone.0146858.
[23] D. S. Ramanathan *et al.*, "Low-frequency cortical activity is a neuromodulatory target that tracks recovery after stroke," (in eng), *Nat Med,* vol. 24, no. 8, pp. 1257-1267, 08 2018, doi: 10.1038/s41591-018-0058-y.